Investigating size effects of complex nanostructures through Young-Laplace equation and finite element analysis

Dingjie Lu, Yi Min Xie, Qing Li, Xiaodong Huang, and Shiwei Zhou'

Citation: Journal of Applied Physics **118**, 204301 (2015); doi: 10.1063/1.4935819
View online: http://dx.doi.org/10.1063/1.4935819
View Table of Contents: http://aip.scitation.org/toc/jap/118/20
Published by the American Institute of Physics

JOURNAL OF APPLIED PHYSICS **118**, 204301 (2015)

Investigating size effects of complex nanostructures through Young-Laplace equation and finite element analysis

Dingjie Lu,[1] Yi Min Xie,[1] Qing Li,[2] Xiaodong Huang,[1] and Shiwei Zhou[1,a)]
[1]*Centre for Innovative Structures and Materials, School of Civil, Environmental and Chemical Engineering, RMIT University, GPO Box 2476, Melbourne 3001, Australia*
[2]*School of Aerospace, Mechanical and Mechatronic Engineering, The University of Sydney, New South Wales 2006, Australia*

(Received 6 August 2015; accepted 3 November 2015; published online 23 November 2015)

Analytical studies on the size effects of a simply-shaped beam fixed at both ends have successfully explained the sudden changes of effective Young's modulus as its diameter decreases below 100 nm. Yet they are invalid for complex nanostructures ubiquitously existing in nature. In accordance with a generalized Young-Laplace equation, one of the representative size effects is transferred to non-uniformly distributed pressure against an external surface due to the imbalance of inward and outward loads. Because the magnitude of pressure depends on the principal curvatures, iterative steps have to be adopted to gradually stabilize the structure in finite element analysis. Computational results are in good agreement with both experiment data and theoretical prediction. Furthermore, the investigation on strengthened and softened Young's modulus for two complex nanostructures demonstrates that the proposed computational method provides a general and effective approach to analyze the size effects for nanostructures in arbitrary shape. © *2015 AIP Publishing LLC*. [http://dx.doi.org/10.1063/1.4935819]

I. INTRODUCTION

When the size of a structure approaches the nanoscale, its mechanical properties such as Young's modulus and strength could significantly increase.[1–6] For instance, both theoretical analysis and experimental measurements have verified that carbon nanotubes possess amazing specific strength (strength-to-weight ratio) amounting to 48 000 kN m/kg, a 200-fold increase in comparison with carbon steel in macro size.[7,8] Such size-dependent effects have received increasing attention as they might have promising applications in lightweight structure, high strength material, catalysis, sensing, and actuating.[9–11]

The enhancement in mechanical properties is mainly attributed to the strong interactions of molecules and their clusters on the material surface when the ratio of surface area to volume becomes extremely large in reduced dimensionality.[1,12,13] With the assumption that surface layers can be superposed and inner substances possess the same elastic properties as bulk material, several analytical methods have been established to quantitatively explain the size effects for nanostructures in terms of Gurtin's surface elasticity theory.[14] The first of such methods is based on a core-shell structure to account for a hardened external surface and has been successfully utilized to explain the dramatic rise of Young's modulus for ZnO nanowire in experiments.[15,16] By employing surface stress and surface elasticity, the sliver nanowire is considered as a composite composed of an inner bulk kernel and a bounding skin under the framework of classical continuum theory, which reasonably explains the remarkable increase of Young's modulus with respect to the decrease of the diameter of a nanowire.[14] Later, a model integrating both the generalized Young-Laplace equation and surface elasticity theories was proposed to essentially predict the softening or stiffening effects on the mechanical properties for nanostructures.[17] Integrated with simple beam theories, this method offers an adequate platform to determine the effective Young's modulus for nano beams.[10,18,19] Though these analytical methods enable the size-dependent properties to be calculated by some explicit formula, they are only applicable to fairly simple structures such as simply supported beams with regular cross section and orthogonal frames. Moreover, the strict restrictions on the boundary conditions and external loadings preclude their applications to complex nanostructures, which are ubiquitous in real scenarios.

An alternative approach to compensating for the insufficiencies of analytical methods is classical molecular dynamics simulation.[20–22] This method offers insights into the exceptional performance of nanomaterials at atomic scope and therefore has been widely used to study surface effects. As it necessitates knowing the motions of each individual particle and their interactions, molecular dynamics simulations are only applicable to ultra-small and highly simplified geometrical models. For a common structure at tens of nanometers in size, molecular dynamics simulation is infeasible as the computational cost would be astronomical due to the enormous constituting particles (e.g., 60×10^6 for a 100 nm gold cubic).[23] To avoid such a prohibitive computational cost, finite element method based approaches are often used.[24] In this method, a two-node surface element is developed to illustrate the strong size dependence of Young's modulus for a 2D structure subjected to pressure in its cavity.[25] To simulate a nanowire beam under large deformation,

a)Author to whom correspondence should be addressed. Electronic mail: shiwei.zhou@rmit.edu.au

a finite element using an absolute nodal coordinate formulation algorithm[26] is employed to account for the strengthening and softening effects.[17,27] To tackle the discontinuities across the interface of two solids for the general deformation in 3D, the level set method[28] and the extended finite element method[29] are integrated.[4,30]

This paper will transfer one of the representative surface effects into non-uniform pressure against the external surface of a complex structure based on the generalized Young-Laplace equation. It will be applicable to the evaluation of the size effects for the nanostructures in any arbitrary shape, which has not been resolved to the best of our knowledge. Considering the fact that these advanced structures can be prototyped by modern nanofabrication technology precisely and efficiently,[31] the work in this field is promising.

The rest of this paper is structured as follows. Firstly the generalized Young-Laplace equation and surface elasticity theory used to describe the size effects at nanoscale is introduced. Then shape-dependent pressure is applied to the surface in order to transfer the size effects into the finite element model. Numerical implementation for a benchmark beam fixed at both ends is elaborated thereafter. Then the influence of surface stiffness and initial surface tension on the effective Young's modulus is discussed. To further demonstrate the capacity of the proposed method, the size effects of two complex structures at nanometer scale are investigated. One is featured with ultra-light and ultra-stiff properties[32] while the other is produced from structural topology optimization[33] for the sake of obtaining maximal stiffness.

II. GENERALIZED YOUNG-LAPLACE EQUATION

According to the surface elasticity theory,[14] the surface stress $\sigma^s_{\alpha\beta}$, a symmetric 2×2 tensor in tangent plane, is given as

$$\sigma^s_{\alpha\beta} = \frac{\partial G\left(\varepsilon^s_{\alpha\beta}\right)}{\partial \varepsilon^s_{\alpha\beta}} + \tau_0 \delta_{\alpha\beta} \quad (\alpha, \beta = 1, 2, 3), \tag{1}$$

where $\varepsilon^s_{\alpha\beta}$ is surface strain tensor, $G(\varepsilon^s_{\alpha\beta})$ is surface energy in the global coordinate system, and $\delta_{\alpha\beta}$ is the Kronecker delta. The initial surface tension is represented by τ_0. Under the assumption that the surface is homogeneous, isotropic, and linearly elastic, the overall surface stress tensor can be expressed as

$$\sigma^s_{\alpha\beta} = \tau_0 + E_s \varepsilon^s_{\alpha\beta}, \tag{2}$$

where E_s is the effective surface stiffness. In accordance with Eq. (2), the stress tensor σ_s in the tangent plane of a surface can be determined as long as the strain is given. Attributed to the size effects, the stress becomes discontinuous at the surface in the normal direction n. It is mathematically expressed as

$$[\sigma^o - \sigma^i] \cdot n = -\nabla_s \sigma^s, \tag{3}$$

where σ^o and σ^i represent the stress tensor in the inner side and outer side of an interface, respectively. The surface divergence of a surface stress tensor is denoted as $\nabla_s \sigma^s$. This formula is the well-known generalized Young-Laplace equation originally used for a fluidic problem.[14] When employed to explain size effects, it gives the fundamental description of the discontinuity of stress tensor across the curved interface surfaces.

For a representative infinitesimal surface element $OABC$ (Fig. 1(a)) defined on a curvilinear coordinate system $Ox_1x_2x_3$ (O is the origin while x_1, x_2, and x_3 are the coordinate axes, and h_1, h_2, h_3 represent curvilinear orthonormal basis vectors), the generalized Young-Laplace equation is substituted into a scalar form along the normal direction of the interface,[34] given as

$$\sigma^o_{33} - \sigma^i_{33} = (\sigma^s_{11}\kappa_1 + \sigma^s_{22}\kappa_2), \tag{4}$$

where σ^o_{33} and σ^i_{33} are the stresses along the outward and inward normal directions of the infinitesimal surface element, respectively. The principal stresses along the edges (OA and OC) and that with an increment of $\partial\sigma^s{}_{11}/\partial x_1 dx_1$ and $\partial\sigma^s{}_{22}/\partial x_2 dx_2$ along the edges (BC and AB) of the tangent plane are illustrated in Fig. 1(a). Note that the shear stress components are neglected in Eq. (4) for simplification. This equation clearly indicates that the stress discontinuity is the linear combination of the principal stresses and curvature in the local curvilinear coordinate system. Accordingly, the principal curvatures κ_1 and κ_2 of the surface element are given as

$$\kappa_1 = \frac{1}{h_1}\frac{\partial h_1}{\partial x_3}, \quad \kappa_2 = \frac{1}{h_2}\frac{\partial h_2}{\partial x_3}. \tag{5}$$

The stress disparities between the inner and outer surfaces are equivalent to surface loads in the normal direction as shown in Fig. 1(b) with red arrows. Fig. 1(c) is a close-up of a load profile for a representative cross section (cut by the black plane in Fig. 1(b)) at the middle of the beam. If these loads are integrated along the boundaries of such a cross section, they are transferred into the non-uniformly distributed pressure against the external surface. For a circular beam without deflection, the line integral equals zero as the principal curvatures at any pair of symmetrical points have the same magnitude but opposite signs (green arrows in Fig. 1(c)). In other words, the size effect induced loads could be cancelled out if the cross section of a beam is rotational symmetry. However, one side of the beam would become convex (concave) if small perturbations are introduced. As a result, the load balance of opposite points on the surface will break, and centripetal or centrifugal loads would occur as shown by the red arrows in Fig. 1(c). The imbalance of surface loads, together with the initial stress τ_0 and the effective surface stiffness E_s, could make the beam stiffer or softer. Such hardening and softening phenomena are the main reasons of size effects and will be numerically investigated for the Young's modulus hereafter.

III. COMPUTATIONAL IMPLEMENTATION

The generalized Young-Laplace equation is well understood and has become the cornerstone for a series of analytical models. But many complex structures featured with

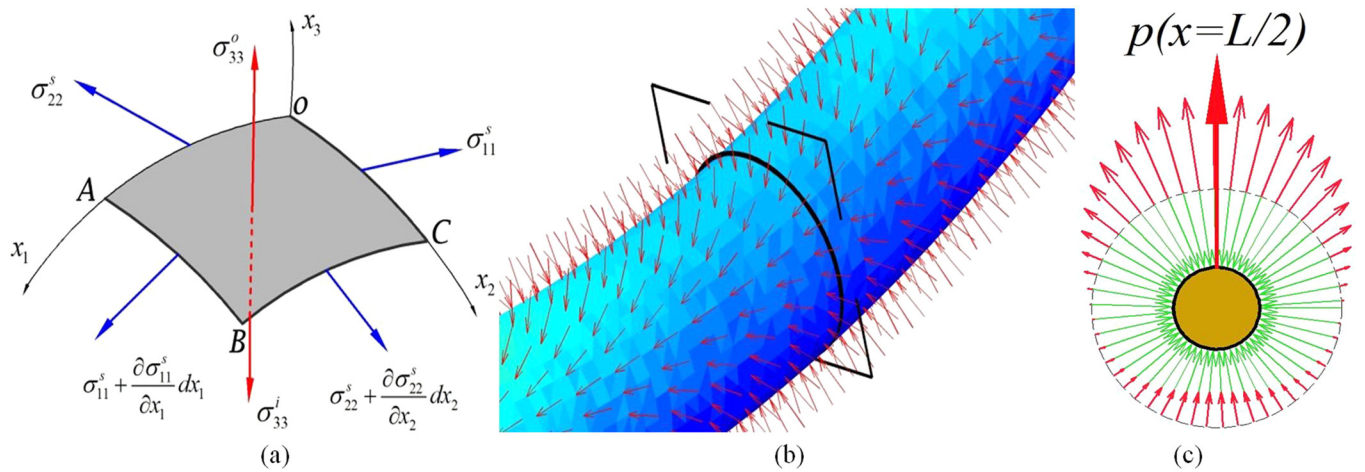

FIG. 1. (a) The schematic of an infinitesimal surface element under stresses caused by size effects; (b) the size-effect-induced pressure along the external surface of a deformed beam; (c) the load profile for a representative cross section at the middle of beam (cut by black plane in Fig. 1(b)).

randomly shaped architectures and unusual loading conditions still require an effective method to determine their size effects. We can, however, use finite element analysis to obtain the effective Young's modulus for these structures. A benchmark of a beam which is fixed at both ends and subjected to a point load at its center is studied first to validate the proposed scheme. The diameter and length of the beam are represented as D and L, respectively (Fig. 2). In terms of Eq. (4), initially there is no surface pressure as the principal curvatures are totally canceled out.

To trigger surface pressure, a concentrated load F is applied downward at the beam center to actuate small but significant initial deflection. Such deformation leads to distributed pressure which bends the beam inversely, sometimes even pushing it upward. In the new configuration, the principal curvatures update the pressure and therefore the just achieved balance is broken. The beam vibrates in such a manner with decreasing amplitude and eventually achieves the final equilibrium state. To be more specific, the iterative process is illustrated in Fig. 2. First, finite element analysis is conducted to simulate the beam deforming from state 1 (grey) to state 2 (cyan) due to load F. Then the principal curvatures of the beam surface at state 2 are calculated to determine the curvature-dependent distributed surface load (blue arrows). Together with load F, this pressure continuously deforms the beam into state 3 (magenta). As a result of further deformation, the surface pressure changes both in magnitude and direction and therefore breaks the balance obtained in the previous step, causing the beam to be transferred to state 4 (green). Because the deflection in the current stage will always be weakened in the next step, the deflection fluctuation attenuates and eventually reaches the balance state (yellow).

A typical convergence process for beams with different diameters is shown in Fig. 3, in which the y-axis denotes the ratio of deflection at the middle point to the beam length while the x-axis gives the iteration step. This figure clearly illustrates that the thinner the beam, the slower it converges. For instance, it takes around 25 steps for $D = 20$ nm to converge while only 5 steps for $D = 50$ nm. Moreover, the initial amplitudes of the thinner beam are remarkably larger than the thicker ones, consistent with the common sense that size effects are more significant at a smaller scale. Specifically, we find that the fluctuation fails to converge for a beam with $D < 3$ nm even though hundreds of iteration steps are attempted. The reason for this failure is attributed to the fact

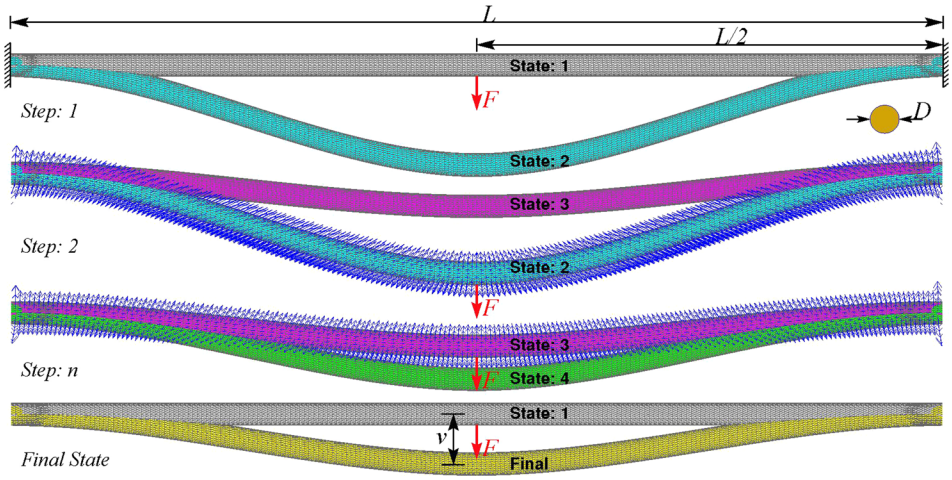

FIG. 2. The iterative simulation process to capture the size-effect-induced pressure for a beam fixed at both ends under concentrated load F at the beam centre.

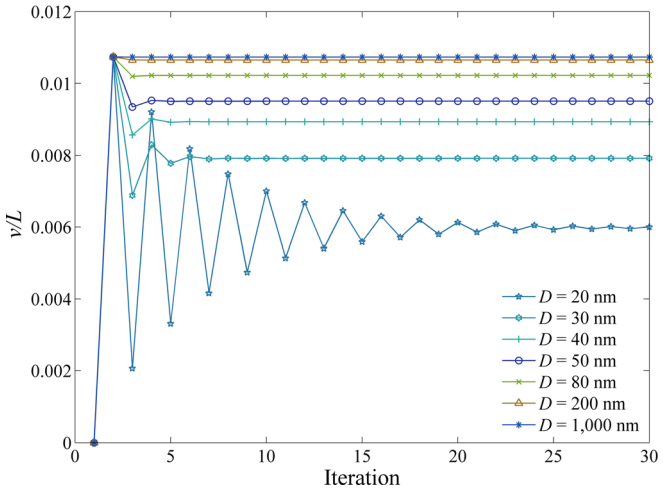

FIG. 3. The magnitude of normalized deflection at the middle point of a beam fixed at both ends versus iteration step.

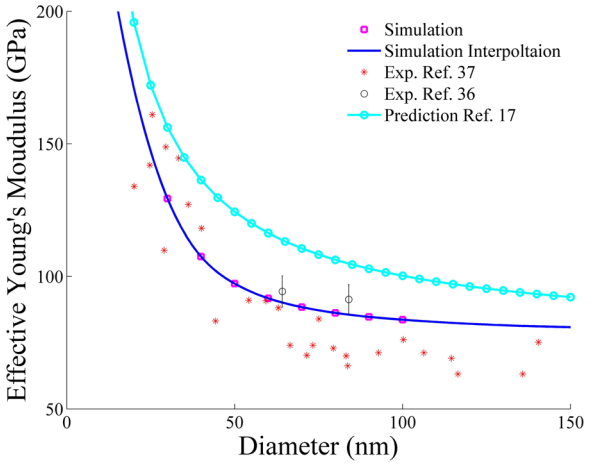

FIG. 4. The effective Young's modulus from an analytical model,[17] experimental data,[36,37] and computational results.

that the surface pressure is extremely large for thin beams, resulting in a non-feasible solution due to the fracture of a beam.

The effective Young's modulus for this simply supported beam undergoing deflection ν can be obtained in accordance with classic Euler-Bernoulli beam theory,[35] given as

$$v_{\max} = \frac{FL^3}{192E^*I}, \tag{6}$$

where v_{max} is the maximal deflection for the same beam subjected to identical loads and supports and $I = \pi D^4/64$ represents the second moment of inertia of a circular cross section. Because the biggest deflection is around $0.1094D$ or $0.0055L$ in the iteration, it is reasonable to use the assumption of small deformation and neglect the axial stress alone the longitudinal direction.[35] Therefore, the effective Young's modulus E^* of the simulated beam can be determined as

$$E^* = \frac{FL^3}{192v_{\max}I}. \tag{7}$$

The blue curve in Fig. 4 is the interpolated effective Young's modulus E^* (denoted by the magenta square markers) for a beam with fixed $D{:}L = 1{:}20$. It clearly demonstrates the surge of E^* as the characteristic size approaches 50 nm. Similar trajectories have been reported in tests, in which a silver nanowire is suspended over a dent and its two ends are tightly clamped onto the substrate. The experimental data[36,37] are represented as red stars and red circular markers (the error bars stand for the acceptable error margins), respectively, in Fig. 4. It is interesting to note, for the similar simply supported beams under the same boundary conditions, the blue curve matches with the experimental data (red stars) reasonably well, especially for a thinner beam with $D < 50$ nm. Moreover, the numerical results are within the error margins for two tests (black circles) with $D = 60$ nm and $D = 79$ nm. Though having the same surface parameters, theoretical prediction[17] represented by the cyan curve with circular marks is, however, notably larger than both the computational results and experimental data. When the beam becomes thicker, the results from computational simulation still perform better than the analytical model although both of them deviate from experimental data.

To demonstrate the superiority of this computational method to theoretic analysis, a complex architecture (yellow parts in Fig. 5(a)) claimed to have ultra large stiffness[32] was simulated herein. This structure is inscribed in a cube with a width of W and all struts have the same circular cross section with diameter D. Though the length of some struts are different, the ratio of its diameter to the width of a cube is fixed to $D{:}W = 1{:}25$. Because the complexity of this structure, an explicit solution based on theoretical analysis[17–19] might not exist. Therefore we have to resort to a computational method for such an irregular structure. Due to structural symmetry, a simple uniaxial pressure test is capable of determining the effective Young's modulus by imposing downward deflection which is equivalent to a strain $\varepsilon = 0.1$ (the deformed structure is depicted by silver color in Fig. 5(a)). With the rational assumption that all bilateral faces have undergone in-plane deformation when the structures are periodically repeated in space, the effective Young's modulus can be determined as

$$E^* = \sigma/\varepsilon, \tag{8}$$

where the stress $\sigma = F/A$ is equal to the reaction force F divided by the area A of the inscribed cube.

For several representative values of surface stiffness E_s and initial surface tension τ_0, the effective Young's modulus E^* of this complex structure is plotted in Fig. 5(b). It is evident that the proposed scheme captures the experimentally observed rising Young's modulus as the diameter is smaller than 10 nm (which is equivalent to a cell with a width of 250 nm). This figure also reveals that the role of surface stiffness is insignificant as a large variation of E_s from 8.7 N/m to 50 N/m merely leads to a marginal difference (shown as the nearly overlapped green and blue lines in the inset). However, the effective Young's modulus is quite sensitive to the change of initial surface tension as shown by the red, pink, and blue curves in Fig. 5(b). A similar finding that E^*

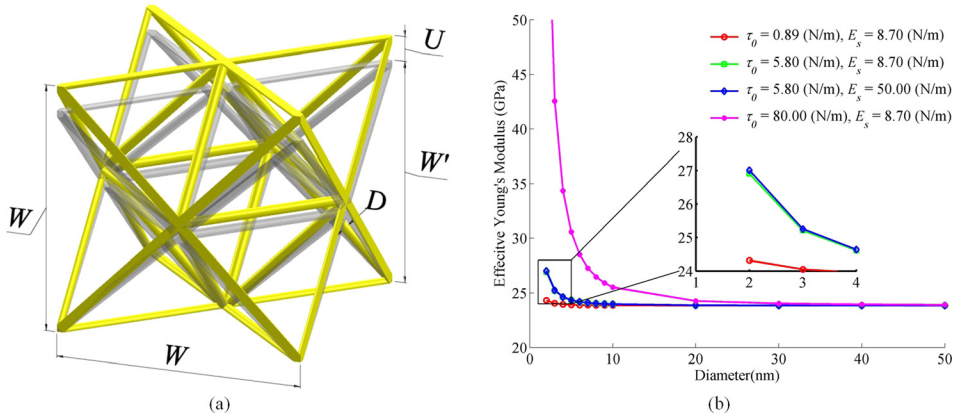

FIG. 5. (a) A complex cubic structure of width W subjected to vertical compression and (b) its effective Young's modulus versus strut diameter D.

is proportional to τ_0 has been reported previously via an analytical model.[10] Because this lattice structure is stretch dominant, its stiffness is much larger than the bending dominant beams in Fig. 4. Therefore it can resist the size-effect-induced pressure more effectively. As a result, the increase of effective Young's modulus is comparably smaller than that in the previous example. Moreover, this structure is likely to alleviate size effects as the critical diameter for the surge of E_s is as small as $D < 10\,\text{nm}$.

To further test this computational method, it is used to retrieve the effective Young's modulus for a cantilever (Fig. 6(a)) which is designed to have the maximal stiffness using structural topology optimization.[33] The ration of height (H), length (L), and width (W) of this beam is $L{:}H{:}W = 6{:}3{:}1$ and the real dimensions are multiplied by 20β (β is a scale factor with the unit of nm). A unit load F is applied at the bottom-left end while the right surface is fixed. Within the linear elastic assumption, the maximal deflection is inversely proportional to the effective Young's modulus.[35] Therefore the effective Young's modulus E^* could be obtained as

$$E^* = \frac{v_{0\max}}{v_{\max}} E_0, \tag{9}$$

where $v_{\max}$ and $v_{0\max}$ denote the maximal deflection with and without the consideration of size effects, and E_0 is the Young's modulus of the bulk material. Several computational tests are conducted with different combinations of surface stiffness E_s and initial surface tension τ_0, all showing a remarkable softening effect as the scale factor $\beta < 10\,\text{nm}$ in Fig. 6(b). A similar softening effect for a cantilever beam with a circular cross section has been found by He *et al.*[17]

The weakened Young's modulus is mainly attributed to the convex shape of the deformed cantilever, which results in a downward pressure. This additional pressure bends the beam with the same direction as the external force F. Thus the deflections are superimposed other than partially offset in previous examples. For this complex cantilever, it is found that both initial surface tension τ_0 and surface stiffness E_s are appropriate to the softened Young's modulus. However, τ_0 plays a more important role than E_s as a moderate increase τ_0 (from $\tau_0 = 0.89\,\text{N/m}$ to $\tau_0 = 5.8\,\text{N/m}$) distinctly changes E^* from the red curve to the green curve, while a considerable rise of E_s (from $E_s = 8.7\,\text{N/m}$ to $E_s = 50\,\text{N/m}$) only slightly changes E^* as shown in the green curve and blue curve in Fig. 6(b).

IV. CONCLUSIONS

In this study, we have proposed a recursive computational method to determine the size effects for nanostructures by integrating finite element analysis with a generalized Young-Laplace equation. One of the representative surface effects is transferred into non-uniformly distributed pressure against the external surface of nanostructures according to Gurtin's surface elasticity theory. Computational results illustrate that this method can well capture the experimentally observed strengthening and softening effects when the characteristic size approaches tens of nanometers. More importantly, the computational method enables the investigation of size effects for complex structures, which are beyond the capability of conventional analytical methods. The first example of a complex structure also reveals the critical size

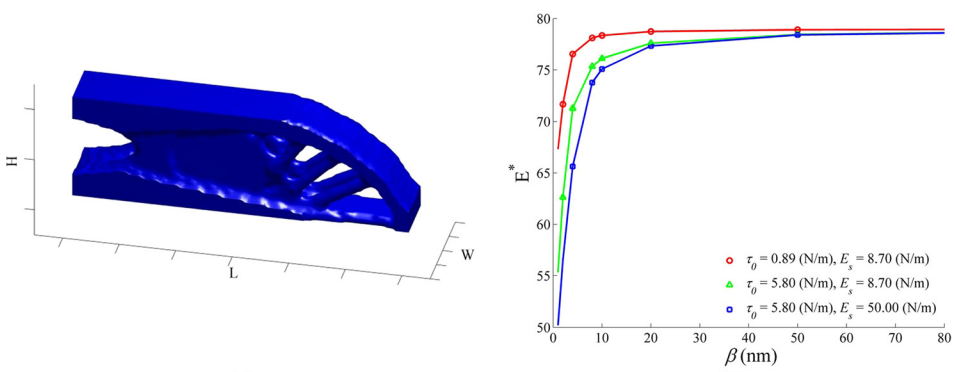

FIG. 6. (a) A complex cantilever with maximal stiffness using structural topology optimization; (b) the effective Young's modulus E^* as a function of scale factor β.

below which the size effects become notable is 20 nm, much smaller than 50 nm of beams with both ends fixed. Parametric studies on the initial surface tension and surface stiffness show that the former is a predominant factor. The weakened Young's modulus is found in a complex cantilever which is produced from structural topology optimization. This computational method also indicates the potential of introducing structural topology optimization into a nano-structure design as two illustrating examples clearly show that size effects are highly dependent on the structural shape and topology at nanoscale.

ACKNOWLEDGMENTS

The work was funded by the Australian Research Council (DE120102906) and the State Key Laboratory of Advanced Design and Manufacturing for Vehicle Body, Hunan University, China, Open Research Fund Program (31415005).

[1]R. C. Cammarata, Prog. Surf. Sci. **46**, 1 (1994).
[2]T. Chen, G. J. Dvorak, and C. C. Yu, Acta Mech. **188**, 39 (2007).
[3]J. Diao, K. Gall, and M. L. Dunn, Phys. Rev. B **70**, 075413 (2004).
[4]M. Farsad, F. J. Vernerey, and H. S. Park, Int. J. Numer. Methods Eng. **84**, 1466 (2010).
[5]P. Sharma, S. Ganti, and N. Bhate, Appl. Phys. Lett. **82**, 535 (2003).
[6]G. Cao and X. Chen, J. Appl. Phys. **102**, 123513 (2007).
[7]M. F. Yu, O. Lourie, M. J. Dyer, K. Moloni, T. F. Kelly, and R. S. Ruoff, Science **287**, 637 (2000).
[8]B. Peng, M. Locascio, P. Zapol, S. Li, S. L. Mielke, G. C. Schatz, and H. D. Espinosa, Nat. Nanotechnol. **3**, 626 (2008).
[9]Y. Jung, K. T. Chu, and S. Torquato, J. Comput. Phys. **223**, 711 (2007).
[10]D. Lu, Y. M. Xie, Q. Li, X. Huang, and S. Zhou, Appl. Phys. Lett. **105**, 101903 (2014).
[11]L. R. Meza, S. Das, and J. R. Greer, Science **345**, 1322 (2014).
[12]A. M. Hodge, J. Biener, J. R. Hayes, P. M. Bythrow, C. A. Volkert, and A. V. Hamza, Acta Mater. **55**, 1343 (2007).
[13]H. F. Zhan and Y. T. Gu, J. Appl. Phys. **111**, 084305 (2012).
[14]M. Gurtin and A. Ian Murdoch, Arch. Ration. Mech. Anal. **57**, 291 (1975).
[15]C. Q. Chen, Y. Shi, Y. S. Zhang, J. Zhu, and Y. J. Yan, Phys. Rev. Lett. **96**, 075505 (2006).
[16]C. Q. Chen and J. Zhu, Appl. Phys. Lett. **90**, 043105 (2007).
[17]J. He and C. M. Lilley, Nano Lett. **8**, 1798 (2008).
[18]X. Q. Feng, R. Xia, X. Li, and B. Li, Appl. Phys. Lett. **94**, 011916 (2009).
[19]R. Xia, X. Q. Feng, and G. F. Wang, Acta Mater. **59**, 6801 (2011).
[20]R. E. Miller and V. B. Shenoy, Nanotechnology **11**, 139 (2000).
[21]V. B. Shenoy, Phys. Rev. B **71**, 094104 (2005).
[22]C. Mi, S. Jun, D. A. Kouris, and S. Y. Kim, Phys. Rev. B **77**, 075425 (2008).
[23]H. S. Park and P. A. Klein, Comput. Methods Appl. Mech. Eng. **197**, 3249 (2008).
[24]D. Lee, X. Wei, M. Zhao, X. Chen, S. C. Jun, J. Hone, and J. W. Kysar, Modell. Simul. Mater. Sci. Eng. **15**, S181 (2007).
[25]W. Gao, S. Yu, and G. Huang, Nanotechnology **17**, 1118 (2006).
[26]A. A. Shabana, *An Absolute Nodal Coordinate Formulation for the Large Rotation and Deformation Analysis of Flexible Bodies* (Department of Mechanical and Industrial Engineering, University of Illinois at Chicago, 1996).
[27]J. He and C. Lilley, Comput. Mech. **44**, 395 (2009).
[28]S. Osher and J. A. Sethian, J. Comput. Phys. **79**, 12 (1988).
[29]N. Moës, J. Dolbow, and T. Belytschko, Int. J. Numer. Methods Eng. **46**, 131 (1999).
[30]J. Yvonnet, H. L. Quang, and Q. C. He, Comput. Mech. **42**, 119 (2008).
[31]C. Sun, N. Fang, D. Wu, and X. Zhang, Sens. Actuators, A **121**, 113 (2005).
[32]X. Zheng, H. Lee, T. H. Weisgraber, M. Shusteff, J. DeOtte, E. B. Duoss, J. D. Kuntz, M. M. Biener, Q. Ge, J. A. Jackson, S. O. Kucheyev, N. X. Fang, and C. M. Spadaccini, Science **344**, 1373 (2014).
[33]X. Huang and Y. M. Xie, *Evolutionary Topology Optimization of Continuum Structures: Methods and Applications* (Willey, 2010).
[34]T. Chen, M.-S. Chiu, and C.-N. Weng, J. Appl. Phys. **100**, 074308 (2006).
[35]J. M. Gere and S. Timoshenko, *Mechanics of Materials* (PWS-KENT Pub. Co., 1990).
[36]Y. Chen, B. L. Dorgan, D. N. McIlroy, and D. Eric Aston, J. Appl. Phys. **100**, 104301 (2006).
[37]G. Y. Jing, H. L. Duan, X. M. Sun, Z. S. Zhang, J. Xu, Y. D. Li, J. X. Wang, and D. P. Yu, Phys. Rev. B **73**, 235409 (2006).